Leveraging self-supervised deep learning to address cross-talks in multi-parameter inversions

Wenlong Wang[*¶], *Yulang Wu*[†¶], *Yanfei Wang*[‡], *George A. McMechan*[§]
[*]*Harbin Institute of Technology,* [†]*University of California, San Francisco,* [‡]*Institute of Geology and Geophysics, Chinese Academy of Sciences,* [§]*The University of Texas at Dallas,* [¶]*These authors contributed equally to this work.*

SUMMARY

Geological structures are typically analyzed using a multi-parameter model (MPM). However, current methods such as multi-parameter full waveform inversion face challenges in accurately determining MPM due to complex inter-parameter crosstalks in the elastic wave equation. To solve this problem, a self-supervised geophysical subsurface imaging approach (SS-GSI) is proposed to leverage multiple independent deep learning networks to predict the MPM based on the migration images and prior models. As a self-supervised learning procedure, the target-oriented datasets are iteratively created by randomly perturbing the inverted models and paired with their migrated images as pseudo-labels. This approach does not require a large number of training samples as in supervised learning algorithms. An important feature of SS-GSI is that the misfit function is independent of seismic data residuals. The data misfit serves only as a validation metric for the accuracy of its predictions. This feature makes SS-GSI immune from crosstalks in multi-parameter inversions. Results from synthetic elastic and anisotropic model simulations demonstrate that SS-GSI outperforms the current state-of-the-art elastic full waveform inversions, providing highly precise and detailed MPM results.

INTRODUCTION

Full-waveform inversion (FWI) (Tarantola, 1986) is capable of generating high-resolution subsurface models by matching predicted seismic data to observed seismic data. However, multi-parameter elastic FWI (EFWI) is usually ill-posed because of the coupling effects between different types of parameters (Virieux and Operto, 2009). Typically, mitigating inter-parameter coupling involves either a hierarchical approach (estimating each type of parameter sequentially) (Prieux et al., 2013; Ren and Liu, 2016), or sophisticated optimization methods that require a true or approximated Hessian (Métivier et al., 2013; Pan et al., 2017).

Deep learning has been widely applied in predicting subsurface models from multiple perspectives. One way is to use supervised deep learning to predict subsurface models from observed seismic data (Araya-Polo et al., 2018), or migration images (Zhang and Gao, 2021) in an end-to-end manner. This type of methods usually suffers from low generalization ability which makes it impractical in real and complicated models. Deep learning can also be applied as a function approximator to re-parameterize the known starting subsurface model to capture the salient features. (Wu and McMechan, 2018, 2019; Zhu et al., 2020; He and Wang, 2021). However, this deep-learning application still requires a seismic data-fitting procedure to update a subsurface model, so it cannot tackle the inter-parameter coupling issues in multi-parameter inversion.

Adaptive feedback CNN-based reflection-waveform inversion (CNN-RWI) (Wu et al., 2021, 2022) predicts the subsurface velocity model from an initial velocity model and the corresponding migration image. The CNN-RWI is classified as self-supervised deep learning, since it iteratively recreates a small set of velocity models as pseudo-labels from the prior velocity model, without the need for massive highly-representative velocity models as in supervised deep learning. As iterations proceed, the velocity models for training (the pseudo-labels) become more representatives, making the CNN prediction more accurate. Inspired by CNN-RWI, we propose self-supervised geophysical subsurface imaging (SS-GSI) to apply mutually independent CNNs to predict MPM, from their initial MPM and the corresponding migration images. Synthetic examples of elastic and anisotropic models illustrate four advantages of the SS-GSI.

THEORY

The workflows of the multi-parameter EFWI and the SS-GSI (Fig. 1) demonstrate synthetic examples for a portion of the Sigsbee elastic model. Both the multi-parameter EFWI and the SS-GSI require observed data (Step 1 in Fig. 1A and 1B, respectively) and the original starting MPM (Step 2 in Fig. 1A and 1B, respectively), as prerequisites for inversion, but for different purposes. The conventional multi-parameter EFWI (Fig. 1A) requires the starting MPM, at the first iteration, to calculate the data residuals and misfits (Step 4 in Fig. 1A) between the predicted data (Step 3 in Fig. 1A) and the observed data (Step 1 in Fig. 1A). Then the multi-parameter gradients, derived from the starting MPM and the data residuals (Step 5 in Fig. 1A), are applied to update the starting MPM (Step 6 in Fig. 1A), to reduce the data residuals and misfits (Step 4 in Fig. 1A) for the next iteration. In the following iterations, the MPM is iteratively updated to gradually reduce the data misfits (Steps 3-6 in Fig. 1A).

For the SS-GSI (Fig. 1B), the observed data are input to the reverse-time migration (RTM) (Baysal et al., 1983; McMechan, 1983; Whitmore, 1983) to estimate the original migration images from the original starting MPM (Step 3 in Fig. 1B). The original starting MPM contains the prior (low-wavenumber) background multi-parameter information whereas the original migration images contain the prior (high-wavenumber) spatial information of the interfaces and reflectors. Both the original starting MPM and the original migration images are input to the mutually independent deep learning models (DL models) (e.g., the workflow in Fig. 1B) to predict the unknown true MPM (Step 4 in Fig. 1B). This CNN prediction step is similar to an end-to-end prediction in most supervised Deep learning

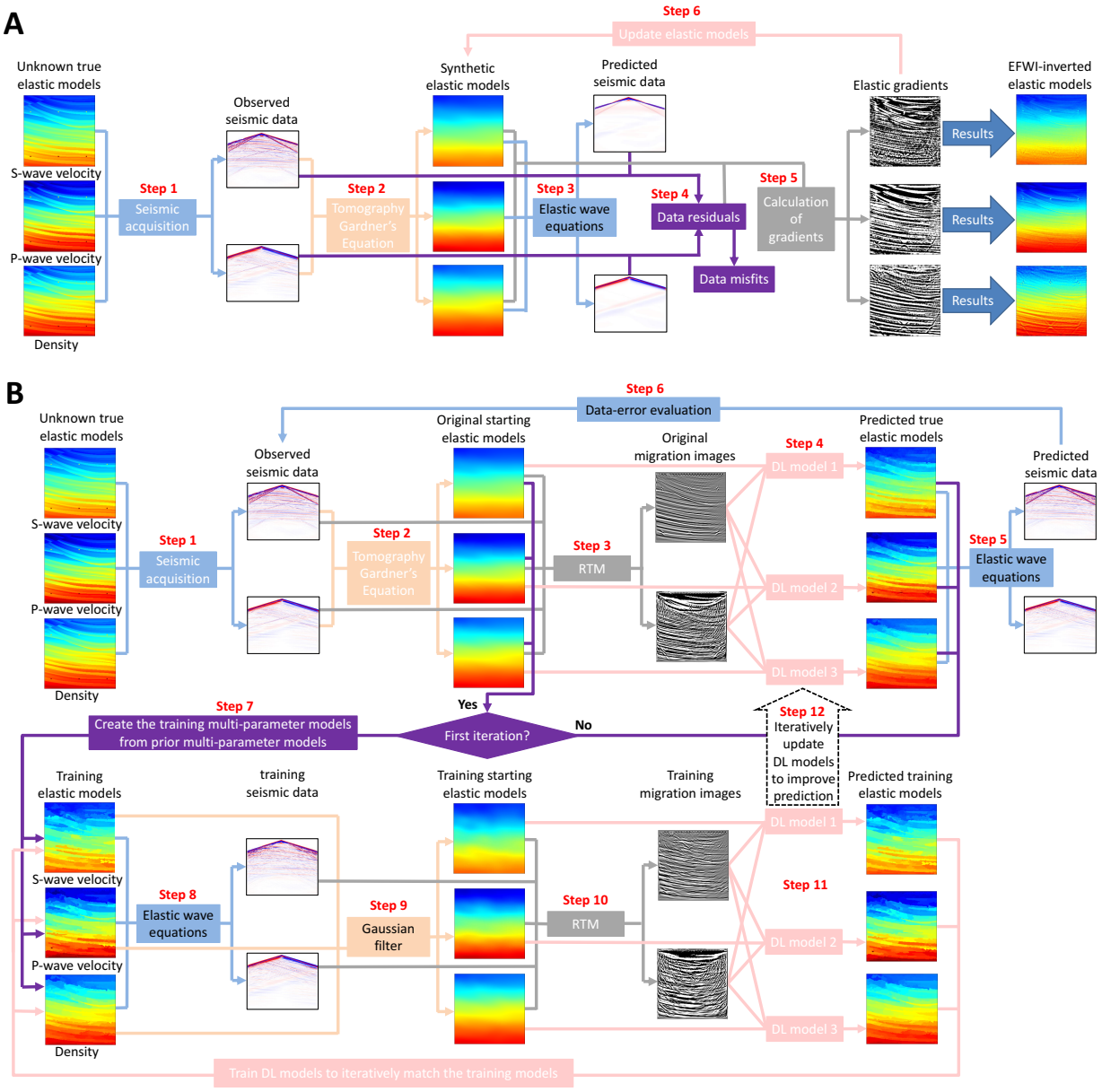

Figure 1: EFWI and SS-GSI pipelines demonstrated by synthetic results on a portion of the Sigsbee elastic model. The arrows with different colors denote the different steps in the pipelines. Each step involves different prerequisites (attached to the ends of the arrows) to generate the products (attached to the heads of the arrows). (A) is the pipeline of the EFWI. (B) is the pipeline of the SS-GSI. The observed seismic data are obtained from the true Sigsbee elastic model via elastodynamic equations. The elastic models (indicated by the 'Step 2' arrows) in (A) and (B) are the original starting elastic models. The elastic gradients in (A) are the sums of the weighted gradients at each iteration. The predicted true and training elastic models in (B) are the CNN-predicted elastic model and one of thirty-two training elastic models at the last iteration, respectively.

applications (Araya-Polo et al., 2018; Lin and Wu, 2018; Yang and Ma, 2019; Wang and Ma, 2020; Zhang and Gao, 2021). The accuracy of the DL models-predicted MPM, evaluated in terms of the data errors (Steps 5 and 6 in Fig. 1B), is used as convergence criteria.

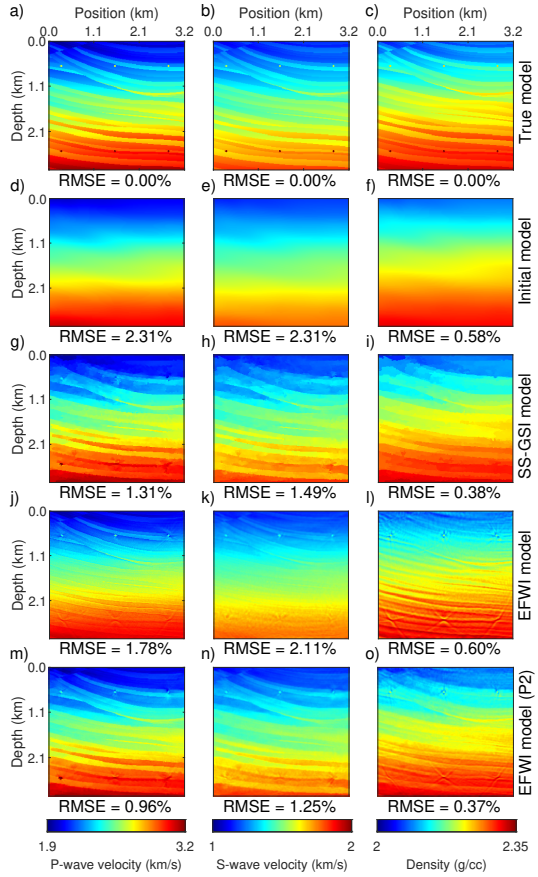

Figure 2: Comparison of the isotropic elastic inversion results on Dataset 1.

CNN architectures

There is no golden rule for the selection of deep learning models for the SS-GSI. Any empirically successful deep learning architecture for image generation and reconstruction, such as the U-Net (Ronneberger et al., 2015), ResNet (He et al., 2016), and so on, can be utilized in SS-GSI to predict the parameter models. As the deep learning models are mutually independent, the architectures of the CNNs could be different, provided that they can fit the training MPM sufficiently accurately. Here, we utilize three mutually independent U-Nets with the same architectures for training and prediction. The architecture of each U-Nets closely resembles the one employed in (Wu et al., 2022), with the only distinction being that the input layer of each U-Nets consists of two components of migration images and an initial parameter model.

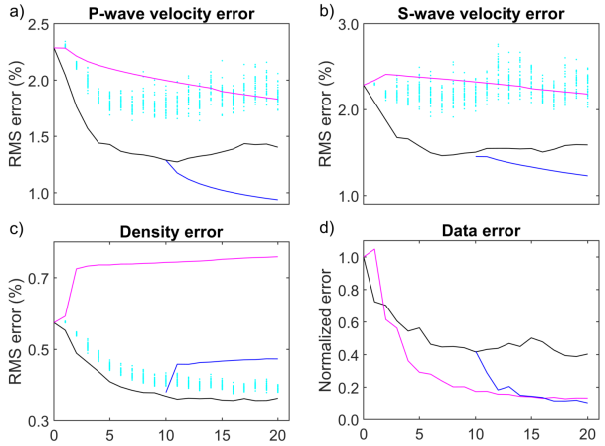

Figure 3: Comparisons of the root-mean-square (RMS) errors of model and data on Dataset 1. The magenta and black lines correspond to the EFWI and SS-GSI methods, respectively, using the initial isotropic elastic models (Fig. 2d-2f) as the starting elastic model. The cyan dots in (a)-(c) correspond to the RMS model errors of the thirty-two training elastic models in the SS-GSI, at each iteration. The blue lines are the EFWI in Pass 2, by using the SS-GSI-inverted elastic models (Fig. 2g-2i) as the starting isotropic elastic models.

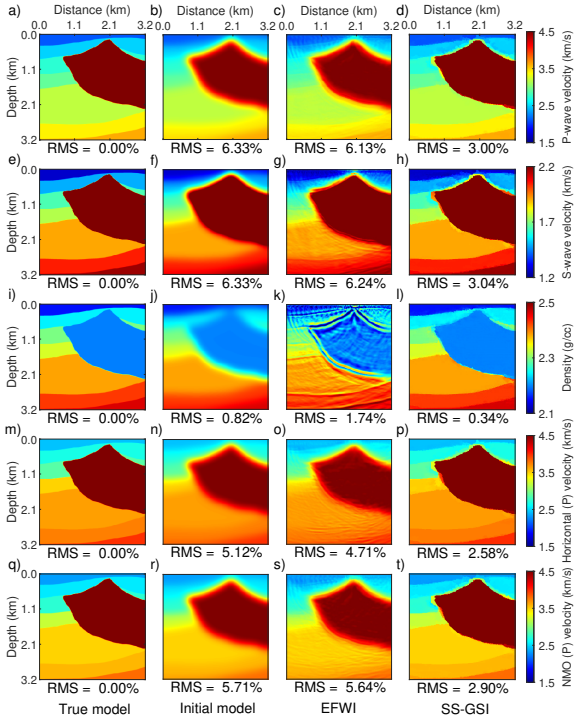

Figure 4: Comparisons of the VTI elastic inversion results on Dataset 2.

SYNTHETIC DATA EXAMPLES

To illustrate the performance of the SS-GSI, an Adam optimization based EFWI (Wang et al., 2021) is compared with the SS-GSI. Inversions are performed and compared on one isotropic elastic model and one anisotropic (VTI) elastic model. The vertical and horizontal extents of the models are 3.2 km, both with a 0.0125 km spatial sampling increment. To simulate the observed data, 25 explosive, Ricker-wavelet sources with a dominant frequency of 20 Hz are spaced every 0.125 km, and 256 receivers are spaced every 0.0125 km. All sources and receivers are at the upper surface. The recording time is 4 s with a 1.0 ms time sampling increment.

Dataset 1: Synthetic tests on the Sigsbee elastic model
The first test is performed on a portion of the Sigsbee isotropic elastic model (Fig. 2) with three parameters to be inverted (P- and S-wave velocity and density). Three inversion results are compared in Fig. 2 and 3. (1) The SS-GSI results after 10 iterations (Fig. 2g-2i); (2) the EFWI result after 20 iterations (Fig. 2j-2l). Both (1) and (2) are initiated by elastic models (Fig. 2d-2f) as the starting models. (3) the elastic models inverted by the EFWI, after 10 iterations, by using the SS-GSI-inverted elastic models (Fig. 2g-2i) as the starting elastic models, as a second pass (P2). Fig. 2 show that the SS-GSI better estimates the elastic models (Fig. 2g-2i) than the EFWI (Fig. 2j-2l) with clearly described formation interfaces.

Dataset 2: Synthetic tests on the Hess anisotropic VTI model
The second test is performed on the Hess anisotropic VTI model with five parameters to be inverted: vertical P- and S-wave velocities, density, NMO P-wave velocity and horizontal P-wave velocity. Fig. 4 shows that the SS-GSI inverts for both the salt body and the sediment layers below the salt body much more accurately than the EFWI does. Because of the high-contrast impedance on the upper and lower boundaries of the salt body, the top surface of the salt body reflects the majority of the energy of the down-going incident waves. Besides, the down-going incident waves transmitted into the salt body create multiple reflections (i.e., multiple reflections created at the upper and lower boundaries of the salt body because of the high-contrast impedance). Matching these complicated multiple reflections is difficult for the EFWI. Therefore, the EFWI cannot invert for the salt body and the regions below it accurately.

In Figures 3 and 5, we compare the model and data errors of SS-GSI and the EFWI results. The EFWI-inverted velocity models have larger errors than SS-GSI-inverted velocity models, partly because EFWI cannot effectively invert for the deeper model by fitting observed reflected data (Yao et al., 2020). In addition, the density errors of EFWI results increase rather than decrease, partly because of the inter-parameter coupling relations, inaccuracy of velocity models, and insensitivity of the density model to the traveltime errors. The model and data errors of the SS-GSI converge to a much lower error level since the mutually independent CNNs adaptively learn to extract and map the features from the migration image (the high-wavenumber interfaces) and from the initial MPM (the low-wavenumber background) to the unknown true MPM. The

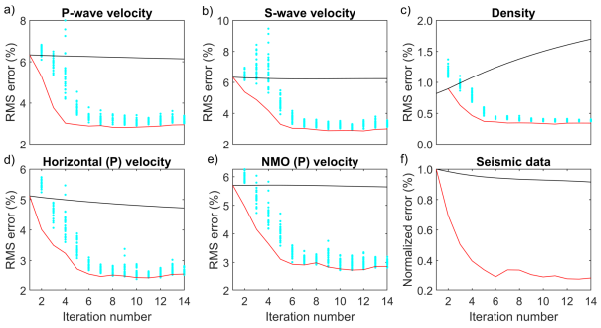

Figure 5: Comparisons of the model and data errors of the Hess VTI model on Dataset 2. The black and red lines correspond to the EFWI and the SS-GSI, using the initial VTI model (in the second column in Fig. 4) as the starting VTI model. The cyan dots in panels (a)-(e) correspond to the RMS model errors of the thirty-two training VTI model, in the SS-GSI, at each iteration.

fluctuation of the data error in accordance with errors of the MPM predicted by the SS-GSI indicates that data errors serve as validation tools for assessing model accuracy since SS-GSI did not minimize the data residuals in a data misfit function.

CONCLUSIONS

The self-supervised geophysical subsurface imaging method (SS-GSI), introduced in this study, effectively addresses the cross-talk issue associated with multi-parameter inversion for two key reasons. Firstly, SS-GSI systematically alleviates sampling biases within the training dataset by dynamically generating an improved training dataset based on the predicted multi-parameter model (MPM). This reduction in sampling bias contributes to more precise predictions. Secondly, each CNN within SS-GSI learns a decoupled mapping from the shared migration images and its assigned initial parameter model to the corresponding true parameter model during the training phase. In contrast, multi-parameter EFWI updates the MPM using gradients contaminated by inter-parameter cross-talks from inaccurate MPM obtained at the previous iteration. Synthetic examples on both elastic (Dataset 1) and anisotropic (Dataset 2) models illustrate that SS-GSI effectively mitigates cross-talk issues, resulting in better predictions of MPM compared to multi-parameter EFWIs.

ACKNOWLEDGMENTS

The research leading to this paper is supported by the National Natural Science Foundation of China under grant NOs.42374142, 12171455 and by the Science Foundation of Heilongjiang Province under grant NO. LH2023D017.